PAPER

A direct sampling method to an inverse medium scattering problem

View the article online for updates and enhancements.

A direct sampling method to an inverse medium scattering problem

Kazufumi Ito[1]**, Bangti Jin**[2] **and Jun Zou**[3]

[1] Department of Mathematics and Center for Research in Scientific Computation,
North Carolina State University, Raleigh, NC, USA
[2] Department of Mathematics and Institute for Applied Mathematics and Computational Science,
Texas A&M University, College Station, TX 77843-3368, USA
[3] Department of Mathematics, The Chinese University of Hong Kong, Shatin, NT, Hong Kong

E-mail: kito@unity.ncsu.edu, btjin@math.tamu.edu and zou@math.cuhk.edu.hk

Abstract
In this work we present a novel sampling method for time harmonic inverse medium scattering problems. It provides a simple tool to directly estimate the shape of the unknown scatterers (inhomogeneous media), and it is applicable even when the measured data are only available for one or two incident directions. A mathematical derivation is provided for its validation. Two- and three-dimensional numerical simulations are presented, which show that the method is accurate even with a few sets of scattered field data, computationally efficient, and very robust with respect to noises in the data.

(Some figures may appear in colour only in the online journal)

1. Introduction

The aim of this work is to numerically study a time harmonic inverse medium scattering problem (IMSP), i.e. imaging inhomogeneous media from near-field measurements [7]. Suppose that a bounded domain Ω in the homogeneous background space $\mathbb{R}^d$ (d = 2, 3) is occupied by some inhomogeneous media. Let $u^{\text{inc}} = e^{ik x \cdot d}$ be an incident plane wave, with the incident direction $d \in \mathbb{S}^{d-1}$ and the wavenumber k. Then the total field u induced by the inhomogeneous media satisfies the Helmholtz equation [7]

$$\Delta u + k^2 n^2(x)u = 0. \tag{1}$$

This equation is generally used to describe time harmonic acoustic wave propagation, where the function $n(x)$ refers to the refractive index, i.e. the ratio of the wave speed in the homogeneous background to that in the local medium at x. We note that the Helmholtz equation (1) also arises in the mathematical modeling of the TM (transverse magnetic) or TE (transverse electric) modes of time harmonic electromagnetic wave propagation in electrically or magnetically inhomogeneous media. Then physically, the function u represents the component

of the electric field E or the magnetic field H in the direction of wave propagation; see [16, pp 72–75] for physical motivations and the appendix for derivation details. We introduce the function $\eta(x) = (n^2(x) - 1)k^2$, which combines the relative refractive index $n^2 - 1$ with the wavenumber k, to characterize the medium inhomogeneity. In particular, $\eta(x)$ vanishes outside the inhomogeneous media Ω. Denote by I the induced current, i.e. $I = \eta u$. Then, the total field u satisfies [7]

$$u = u^{\text{inc}} + \int_\Omega G(x, y)I(y)\, \mathrm{d}y, \tag{2}$$

where $G(x, y)$ is the fundamental solution for the open field and given by

$$G(x, y) = \begin{cases} \dfrac{\mathrm{i}}{4}H_0^1(k|x - y|), & \mathrm{d} = 2, \\[2mm] \dfrac{1}{4\pi}\dfrac{\mathrm{e}^{-ik|x-y|}}{|x - y|}, & \mathrm{d} = 3, \end{cases}$$

where the function H_0^1 refers to the zeroth-order Hankel function of the first kind. By multiplying both sides of equation (2) by η, we arrive at the following second-kind integral equation for the induced current I:

$$I(x) = \eta\, u^{\text{inc}} + \eta \int_\Omega G(x, y)I(y)\, \mathrm{d}y. \tag{3}$$

Let $u^{\text{s}} \equiv u - u^{\text{inc}}$ be the scattered field. Then, the IMSP is to retrieve the shape of the medium scatterer Ω and its distribution η from noisy measurements of the scattered field u^{s} on a curve Γ (d = 2) or surface Γ (d = 3), corresponding to one or multiple incident fields [2, 7, 10]. The reliable yet efficient extraction of such information is of great significance in analyzing acoustic/electromagnetic wave propagation.

We shall present a novel direct sampling method to get a stable and accurate approximation to the shape of the scatterers, or equivalently the support of the inhomogeneity coefficient $\eta = (n^2 - 1)k^2$. It is based on a scattering analysis and involves only computing the inner product of the measured scattered field u^{s} with fundamental solutions located at the sampling points over the measurement curve/surface Γ. The method is strictly direct and does not use any matrix operations, and its implementation is very straightforward. Our numerical experiments indicate that it can provide an accurate and reliable estimate of the support of the unknown scatterers/coefficient η, even in the presence of a fairly large amount of noises in the measured data. Hence, it can serve as an effective yet simple computational alternative to existing tools for locating a reliable approximate position of the unknown scatterers, which can then be used as the initial guess in any existing method [2, 10, 17] for further refinement to get a more accurate estimate of the scatterer support and the inhomogeneity distribution.

The proposed method uses a sampling-type technique, see [13] for an overview of related strategies, and its flavor closely resembles *multiple signal classification* (MUSIC) [8, 9, 15, 11, 4] and the *linear sampling method* (LSM) [6, 12, 3]. The relation between MUSIC and the LSM was addressed in [5]. Our method differs significantly from these two existing techniques. Firstly, it requires only a few (e.g., one or two) incident waves for reconstructing the location of scatterers/inhomogeneities, whereas the latter two require the full map (multi-static response matrix/far-field operator). Secondly, our method does not perform any matrix operations, such as eigenvalue decomposition or projection onto the noise space in MUSIC or solving ill-posed linear integral equations in the LSM, and thus is computationally inexpensive. Lastly, the noise is treated directly, and thus the method is highly tolerant to noise.

2. New sampling method

In this section, we develop a novel direct sampling method to determine the shape of the scatterers/inhomogeneities. The derivation is carried out for a circular curve/spherical surface Γ. It uses the fundamental solution $G(x, x_p)$ associated with the Helmholtz equation in the homogeneous background:

$$\Delta G(x, x_p) + k^2 G(x, x_p) = -\delta(x - x_p), \tag{4}$$

where $\delta(x - x_p)$ refers to the Dirac delta function located at the point $x_p \in \Omega_\Gamma$ (the domain enclosed by Γ). By multiplying both sides of (4) by the conjugate $\overline{G}(x, x_q)$ of the fundamental solution $G(x, x_q)$ and then integrating over the domain Ω_Γ, we derive

$$\int_{\Omega_\Gamma} (\Delta G(x, x_p) + k^2 G(x, x_p)) \overline{G}(x, x_q) \, dx = -\overline{G}(x_p, x_q). \tag{5}$$

Next we consider equation (4) with $x_q \in \Omega_\Gamma$ in place of x_p, and take its conjugate. Then by multiplying both sides of the resulting equation by $G(x, x_p)$ and integrating over the domain Ω_Γ, we obtain

$$\int_{\Omega_\Gamma} (\Delta \overline{G}(x, x_q) + k^2 \overline{G}(x, x_q)) G(x, x_p) \, dx = -G(x_p, x_q). \tag{6}$$

Using integration by parts for the terms involving Laplacians in (5)–(6), we readily deduce

$$G(x_p, x_q) - \overline{G}(x_p, x_q) = \int_\Gamma \left[\overline{G}(x, x_q) \frac{\partial G(x, x_p)}{\partial n} - G(x, x_p) \frac{\partial \overline{G}(x, x_q)}{\partial n} \right] ds. \tag{7}$$

Next we approximate the right-hand side of identity (7) by means of the Sommerfeld radiation condition for the Helmholtz equation, i.e.

$$\frac{\partial G(x, x_p)}{\partial n} = ik G(x, x_p) + \text{h.o.t.}$$

Thus, we use the following approximations:

$$\frac{\partial G(x, x_p)}{\partial n} \approx ik G(x, x_p) \quad \text{and} \quad \frac{\partial \overline{G}(x, x_q)}{\partial n} \approx -ik \overline{G}(x, x_q),$$

which are valid if the points x_p and x_q are not close to the boundary Γ. Consequently, we arrive at the following approximate relation:

$$\int_\Gamma \{ ik G(x, x_p) \overline{G}(x, x_q) + ik \overline{G}(x, x_q) G(x, x_p) \} \, ds \approx 2i \Im(G(x_p, x_q)),$$

i.e.

$$\int_\Gamma G(x, x_p) \overline{G}(x, x_q) ds \approx k^{-1} \Im(G(x_p, x_q)). \tag{8}$$

Now, we consider a sampling domain $\widetilde{\Omega}$ that contains the scatterer support Ω. To motivate the new method, we divide the domain $\widetilde{\Omega}$ into a set of small elements $\{\tau_j\}$. Then by using the rectangular quadrature rule, we arrive at the following simple approximation from the integral representation (2):

$$u^s(x) = \int_{\widetilde{\Omega}} G(x, y) I(y) \, dy \approx \sum_j w_j G(x, y_j), \tag{9}$$

where the point y_j is in the jth element τ_j, and the weight w_j is given by $w_j = |\tau_j| I(y_j)$, with $|\tau_j|$ being the volume of the element τ_j. Since the induced current I vanishes identically outside the support Ω, the summation in (9) is actually only over those elements intersecting with Ω. We remark that the support Ω may consist of several separated subregions, each of

which is occupied by a different physical medium. By standard elliptic regularity theory, the induced current $I = \eta u$ is smooth in each subregion of the same physical medium. Therefore, according to classical approximation theory [14, 18], the approximation in (9) can be made arbitrarily accurate by refining the elements $\{\tau_j\}$. It also works for the general refractive index $n(x)$ as long as it is regular in each subregion (e.g., piecewise smooth media that are frequently encountered in applications). Nonetheless, we reiterate that relation (9) serves only the goal of motivating our method, and will not be needed in the implementation. Physically, (9) also admits an interesting interpretation: the scattered field u^s at any fixed point $x \in \Gamma$ can be regarded as a weighted average of that due to the point scatterers located at $\{y_j\}$ within the true scatterer Ω.

Multiplying both sides of (9) by $\overline{G}(x, x_p)$ for any point x_p that lies in the sampling domain $\widetilde{\Omega}$, then integrating over the boundary Γ and using (8), we obtain the following approximate relation:

$$\int_\Gamma u^s(x)\, \overline{G}(x, x_p)\, \mathrm{d}s \approx k^{-1} \sum_j w_j \Im(G(y_j, x_p)). \tag{10}$$

Relation (10) is valid under the premises that the point scatterers $\{y_j\}$ and the sampling points $\{x_p\}$ are far apart from the measurement surface Γ, and the elements $\{\tau_j\}$ are sufficiently refined.

Relation (10) underlies the essential idea of our new method. We observe directly that if a point x_p is close to some physical point scatterer located at $y_j \in \Omega$, then $G(y_j, x_p)$ is nearly singular and takes a very large value; hence, it contributes significantly to the summation in (10). Conversely, if x_p is far away from all physical point scatterers, then the sum will be very small due to the decay property of the fundamental solution $G(x, y)$.

These facts lead us to the following index function for any point $x_p \in \widetilde{\Omega}$:

$$\Phi(x_p) = \frac{|\langle u^s(x), G(x, x_p)\rangle_{L^2(\Gamma)}|}{\|u^s(x)\|_{L^2(\Gamma)} \|G(x, x_p)\|_{L^2(\Gamma)}}.$$

In practice, if a point x_p satisfies $\Phi(x_p) \approx 1$, then it is most likely within the scatterer support Ω according to the preceding discussions, whereas if $\Phi(x_p) \approx 0$, then the point x_p likely lies outside the support. Compared with MUSIC and the LSM, the index $\Phi(x_p)$ provides the likelihood of the point x_p lying within Ω and hence probably also the coefficient distribution η. The index Φ involves only evaluating the free-space fundamental solution and its inner product with the measured data u^s; thus, it is computationally very inexpensive. Also, the data noise enters the index Φ through the integration of the measured data u^s on the boundary Γ and no unstable matrix inversion as in the LSM is required. Note that the energy of the (random) noise is expected to be equally distributed in all Fourier modes, whereas the fundamental solution $G(x, x_p)$ is very smooth on the curve/surface Γ and concentrates on only low-frequency Fourier modes. Consequently, the high-frequency modes (i.e. noises) in the noisy data are roughly orthogonal to $G(x, x_p)$ and contribute little to the index function Φ. Hence, the method should be robust with respect to the noise, which is confirmed by our subsequent numerical experiments.

3. Numerical experiments

We shall present several examples to illustrate the accuracy of our method for determining the scatterers from both exact and noisy data. We denote the wavelength by $\lambda = 1$, and the wavenumber k is 2π. In 2D examples, unless otherwise specified, one incident direction
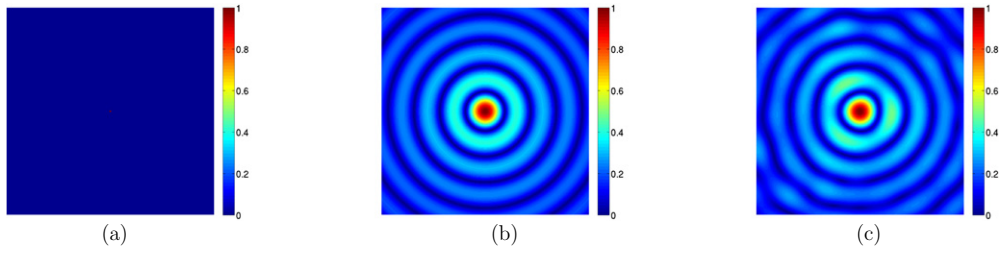
Figure 1. Numerical results for example 1: (a) true scatterer, (b) reconstruction for exact data and (c) reconstruction for noisy data with $\varepsilon = 20\%$.

$d = \frac{1}{2}(1, 1)^{\mathrm{T}}$ is employed, and the scattered field u^{s} is measured at 30 points uniformly distributed on a circle of radius 5λ. The noisy data u^{s}_{δ} are generated pointwise by the formula

$$u^{\mathrm{s}}_{\delta}(x) = u^{\mathrm{s}}(x) + \varepsilon\zeta \max_{x} |u^{\mathrm{s}}(x)|,$$

where ε refers to the relative noise level, and both real and imaginary parts of the noise ζ follow the standard normal distribution. The index Φ is normalized so that its maximum value is 1. The sampling domain $\widetilde{\Omega}$ is fixed at $[-2\lambda, 2\lambda]^2$, which is divided into small squares of equal width $h = 0.01\lambda$. The index Φ as an estimate to the coefficient η will be displayed.

The first example shows the method for one single point scatterer, which provides some insights into the mechanism of the index Φ.

Example 1. The example considers one square scatterer of width 0.02λ located at the origin. The coefficient η of the scatterer is 1.

The numerical results are shown in figure 1. We observe that for sampling points close to the physical scatterer at the origin, the index Φ is relatively large; otherwise, it takes relatively small values. Hence, it does provide an accurate and reliable indicator for the location of the scatterer. The presence of $\varepsilon = 20\%$ noise in the measured data only marginally affects the shape of the index Φ, concurring with the intuitive explanations in section 2. Therefore, the method is very robust to noises.

The second example illustrates the method for two separate scatterers.

Example 2. We consider two square scatterers of side length 0.3λ. The coefficient η in both regions is 1. The following two cases are investigated.

 (a) The two scatterers are located at $(-0.8\lambda, -0.7\lambda)$ and $(0.3\lambda, 0.8\lambda)$, respectively.
 (b) The two scatterers are located at $(-0.25\lambda, 0)$ and $(0.25\lambda, 0)$, respectively.

The two scatterers in example 2(a) are well apart from each other. The recovery of the locations of the scatterers is quite satisfactory, noting the fact that we have just used one incident field; see figure 2, where two distinct scatterers are observed for both exact data and the data with $\varepsilon = 20\%$ noise.

The two scatterers in example 2(b) stay very close to each other, less than one half of the wavelength ($\lambda/2$) in distance, which is known to be rather challenging for numerical reconstruction. Nonetheless, the estimate of the location of the scatterers (cf figure 3) is still very impressive, especially by noting the fact that only one incident field was employed. In particular, the method allows us to distinguish two scatterers of the distance less than $\lambda/2$, the physical resolution limit. However, the origin of such a reconstruction strength remains elusive. Furthermore, the two scatterers are still well separated, with their locations correctly
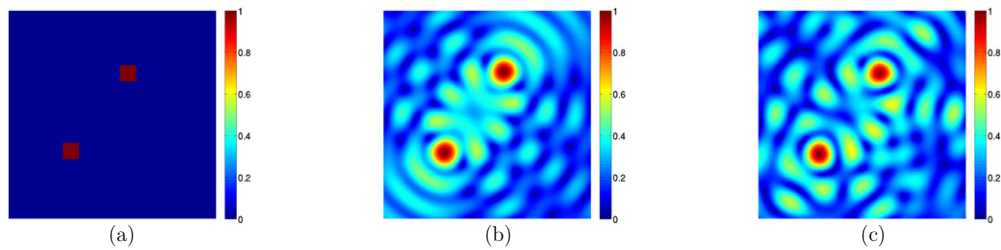
Figure 2. Numerical results for example 2(a): (a) true scatterer, (b) reconstruction for exact data and (c) reconstruction for noisy data with $\varepsilon = 20\%$.
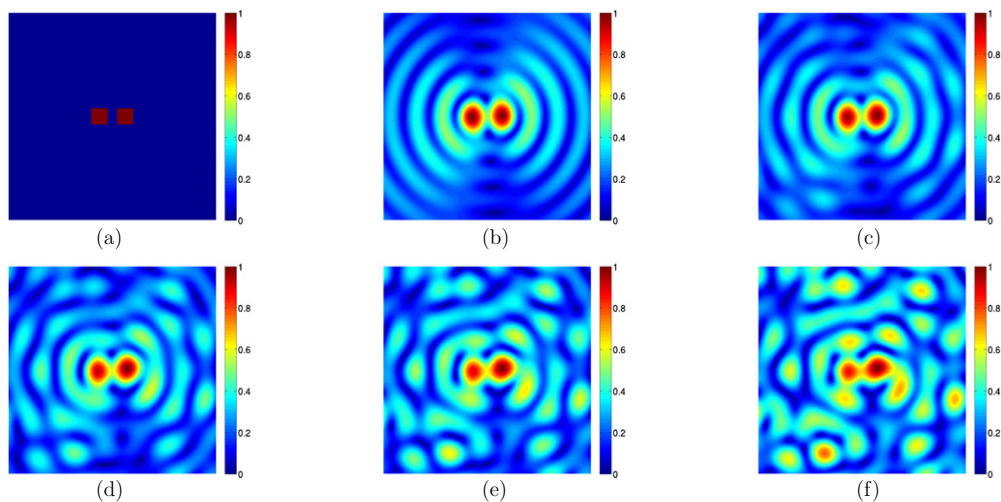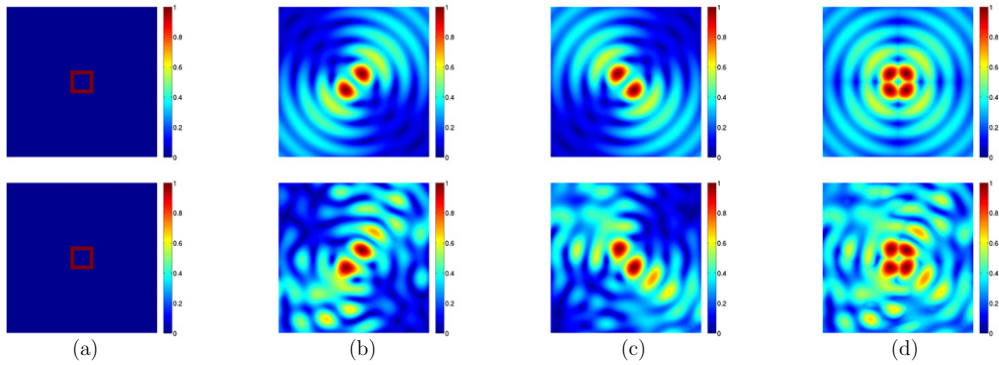

Figure 3. Numerical results for example 2(b): (a) true scatterer, (b) reconstruction for exact data and (c)–(f) reconstructions for noisy data with $\varepsilon = 10\%$–40%, respectively.

estimated, for up to $\varepsilon = 30\%$ noise in the data. In the case of very high noise levels, e.g., $\varepsilon = 40\%$, the estimate tends to connect the supports of the two separate scatterers, and also some spurious modes have emerged in the estimate.

Compared with the case of one point scatterer in example 1, the size of the estimated scatterer support here also agrees well with that of the true one. This is attributed to collective contributions of neighboring pixels, thereby further illuminating the mechanism of the method. However, due to the ill-posed nature of the IMSP and the oscillating behavior of the fundamental solution, the estimate is not free from small spurious oscillations, although the overall profile stands out clearly. This observation is also valid for other examples. In practice, one may use the estimate from the index Φ as an initial guess for other more expensive but more accurate methods, e.g., the regularized least-squares, Gauss–Newton method or contrast source inversion [2, 10, 17], to achieve an enhanced resolution.

Next we consider a ring-shaped scatterer.

Example 3. The scatterer is one ring-shaped square located at the origin, with the outer and inner side lengths being 0.6λ and 0.4λ, respectively. The coefficient η of the scatterer is 1. Two incident directions $d_1 = \frac{1}{\sqrt{2}}(1, 1)^{\mathrm{T}}$ and $d_2 = \frac{1}{\sqrt{2}}(1, -1)^{\mathrm{T}}$ are considered.

Figure 4. Numerical results for example 3: (a) true scatterer; (b), (c) and (d), reconstructions respectively for the incident direction $d_1 = \frac{1}{\sqrt{2}}(1, 1)^{\mathrm{T}}$ and $d_2 = \frac{1}{\sqrt{2}}(1, -1)^{\mathrm{T}}$, and both directions d_1 and d_2. The first and second rows are respectively for the exact data and noisy data with $\varepsilon = 20\%$.

The ring-shaped scatterer represents one of the most challenging objects to resolve, and it is highly nontrivial even with multiple data sets, especially noting the fact that the ring has a very small thickness. It is observed from panels (b) and (c) of figure 4 that one single incident wave is insufficient to recover the ring structure, and only some parts of the ring can be resolved, depending on the incident direction d. Hence, we add one more incident wave to yield sufficient information. In order to fully utilize multiple data sets, we extend the index function Φ as follows:

$$\Phi(x_p) = \max_i \{\Phi_i(x_p)\} \quad \forall x_p \in \widetilde{\Omega},$$

where Φ_i refers to the index function for the ith data set. The results with the exact and $\varepsilon = 20\%$ noise in the data are shown in panel (d) of figure 4. It is observed that with just two incident waves, the method can provide a quite reasonable estimate of the ring shape. The estimate remains very stable for up to $\varepsilon = 20\%$ noise in the data.

The last example shows the feasibility of the method for three-dimensional problems.

Example 4. We consider two cubic scatterers of width $\frac{2}{5}\lambda$ centered at $\left(\frac{2}{5}\lambda, \frac{3}{10}\lambda, \frac{3}{10}\lambda\right)$ and $\left(-\frac{2}{5}\lambda, \frac{3}{10}\lambda, \frac{3}{10}\lambda\right)$, respectively. One single incident field with direction $d = \frac{1}{\sqrt{3}}(1, 1, 1)^{\mathrm{T}}$ is used, and the coefficient η of the scatterers is taken to be 1. The scattered field u^s is measured at 600 points uniformly distributed on the surface Γ of a cube of width 5λ.

This example is challenging since the distance between two scatterers is $\frac{2}{5}\lambda$ and is very close. For the simulation, we take the sampling domain $\widetilde{\Omega}$ for evaluating the index Φ to be $\left[-\frac{3}{2}\lambda, \frac{3}{2}\lambda\right]^3$. The problem is discretized with a mesh size $\frac{1}{10}\lambda$. The numerical results are shown in figure 5, where each row represents a cross-sectional image along the second coordinate axis x_2. We observe that the support estimated by the index Φ agrees excellently with the exact one, and away from the boundary of the true scatterers, the magnitude of Φ decreases quickly. The presence of $\varepsilon = 20\%$ data noise seems to cause no obvious deterioration of the accuracy of the index Φ as compared to that for exact data. Lastly, we would like to point out that the measurement surface Γ here is not spherical as was utilized in the derivation of the index function Φ. Hence, the method is applicable to general geometries.
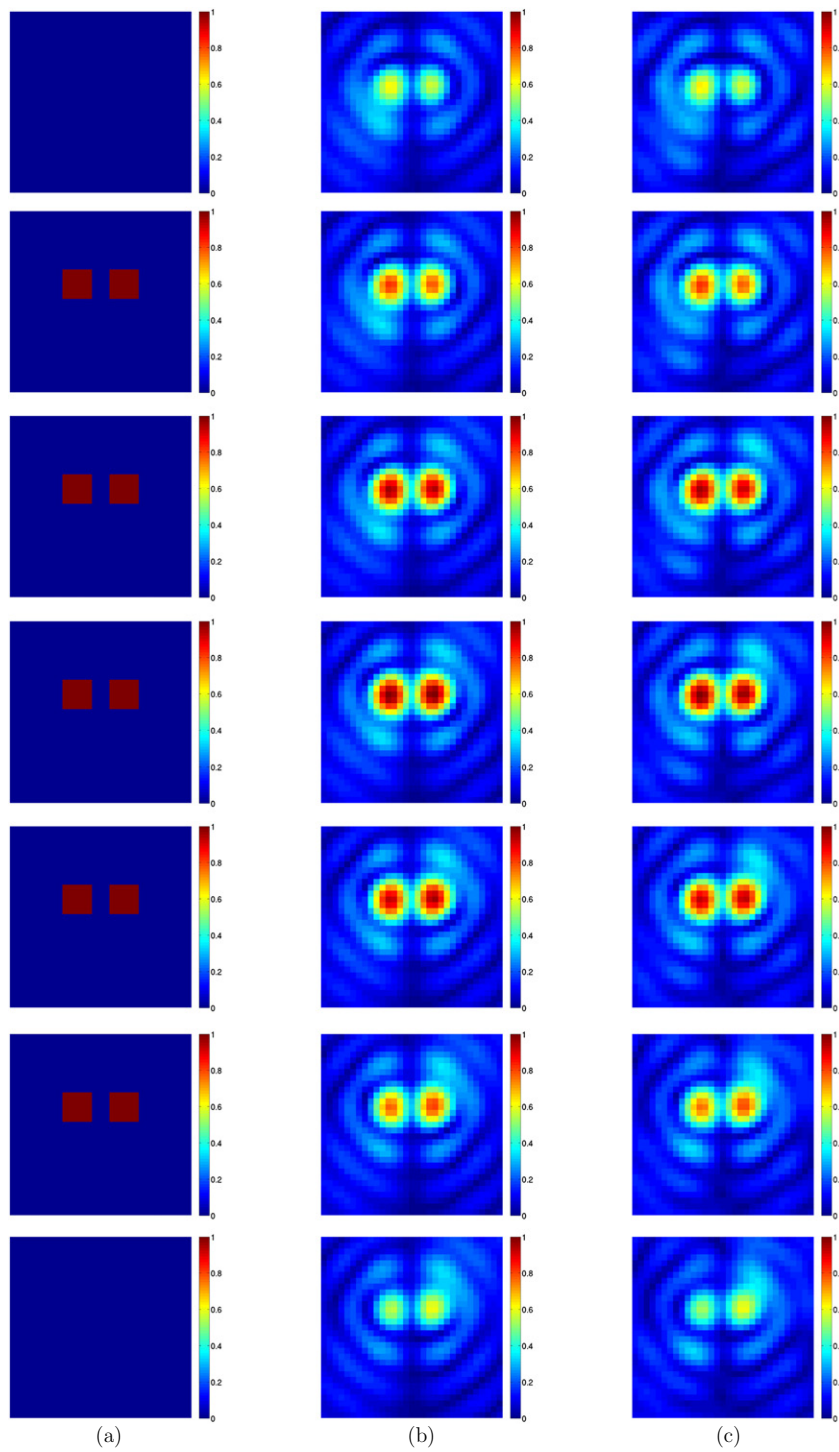
Figure 5. Numerical results for example 4: (a) true scatterer, (b) reconstruction for exact data and (c) reconstruction for noisy data with $\varepsilon = 20\%$. From top to bottom are cross-sectional images for $x_2 = 0, \frac{1}{10}\lambda, \frac{2}{10}\lambda, \ldots, \frac{6}{10}\lambda$.

4. Conclusions

We have presented a novel direct sampling method for inverse medium scattering problems, applicable even to few scattered field data. It involves computing only the inner product of the scattered field with fundamental solutions located at sampling points and hence it is strictly direct. Numerically, it does not require any matrix operations like solving ill-posed integral equations or performing eigenvalue decompositions as most existing techniques do. The experimental results indicate that it can provide an accurate estimate of the scatterer support from the measured data corresponding to only one or two incident directions, and it is also very robust to data noise.

In this preliminary study, we have focused on the direct sampling method. It is natural to use the estimate obtained from the method as an initial guess for other existing methods, e.g., the Tikhonov regularization, Gauss–Newton method or contrast source inversion [2, 10, 17], which are more expensive yet more accurate, so as to obtain images with an enhanced resolution. We would also like to mention that the method might also be applied to other interesting scattering scenarios, e.g., scattering from lines (cracks), far-field measurements and multiple frequencies, which can often provide additional information on the scattering medium. These extensions and their mathematical analysis are ongoing.

Acknowledgments

Appendix A. Deriving the models for TM and TE modes

In this appendix, we show that the Helmholtz equation (1) arises also in the TM and TE modes in time harmonic electromagnetic wave propagation. Recall that, in the absence of interior sources, the Maxwell system for time harmonic waves reads [1, p 57;7]

$$\begin{cases} \operatorname{curl} \boldsymbol{H} = (-\mathrm{i}\omega\epsilon + \sigma)\boldsymbol{E}, \\ \operatorname{curl} \boldsymbol{E} = \mathrm{i}\omega\mu\boldsymbol{H}, \\ \operatorname{div}(\epsilon\boldsymbol{E}) = 0, \\ \operatorname{div}(\mu\boldsymbol{H}) = 0, \end{cases} \tag{A.1}$$

where the vector fields $\boldsymbol{H}$ and $\boldsymbol{E}$ denote the magnetic and electric fields, respectively, the constant ω is the angular frequency, and the functions ϵ, σ and μ refer to electrical permittivity, electrical conductivity and magnetic permeability of the medium, respectively.

A.1. TM waves

For the TM mode, we set $\boldsymbol{H} = (H_x(x, y), H_y(x, y), 0)^{\mathrm{T}}$ and $\boldsymbol{E} = (0, 0, E_z(x, y))^{\mathrm{T}}$. Then the Maxwell system (A.1) reduces to

$$\operatorname{curl} \widetilde{\boldsymbol{H}} = (-\mathrm{i}\omega\epsilon + \sigma)E_z, \qquad \operatorname{curl} E_z = \mathrm{i}\omega\mu\widetilde{\boldsymbol{H}}, \qquad \operatorname{div}(\mu\widetilde{\boldsymbol{H}}) = 0,$$

with $\widetilde{\boldsymbol{H}} = (H_x(x, y), H_y(x, y))^{\mathrm{T}}$. By eliminating $\widetilde{\boldsymbol{H}}$, we arrive at

$$\operatorname{curl}(\mu^{-1}\operatorname{curl} E_z) - (\omega^2\epsilon + \mathrm{i}\omega\sigma)E_z = 0.$$

Suppose that the medium is nonmagnetic, i.e. $\mu = \mu_0$, the constant in the background medium. Then we have div $\widetilde{H} = 0$ and $\mathrm{curl}^2 = -\Delta$, which imply

$$\Delta E_z + (\omega^2 \epsilon \mu_0 + \mathrm{i}\omega\sigma\mu_0)E_z = 0.$$

Let $k = \omega/c_0$, $c_0 = \frac{1}{\sqrt{\epsilon_0\mu_0}}$ and $c = \frac{1}{\sqrt{\epsilon\mu_0}}$, where ϵ_0 is the electric permittivity in the background medium, then we get $\omega^2\epsilon\mu_0 = k^2 c_0^2/c^2$. Hence, in the case of $\sigma = 0$, the desired model (1) follows directly by setting $n = c_0/c$. Since the electrical permittivity ϵ can be spatially varying, the model can appropriately describe electrically inhomogeneous media. Generally, one may take a complex-valued refraction index n to accommodate the presence of (possibly also spatially varying) conductivity σ.

A.2. *TE waves*

For the TE mode, we set $\boldsymbol{E} = (E_x(x, y), E_y(x, y), 0)^{\mathrm{T}}$ and $\boldsymbol{H} = (0, 0, H_z(x, y))^{\mathrm{T}}$. Then the Maxwell system (A.1) reduces to

$$\mathrm{curl}\, H_z = (-\mathrm{i}\omega\epsilon + \sigma)\widetilde{\boldsymbol{E}}, \qquad \mathrm{curl}\, \widetilde{\boldsymbol{E}} = \mathrm{i}\omega\mu H_z, \qquad \mathrm{div}(\epsilon\widetilde{\boldsymbol{E}}) = 0,$$

with $\widetilde{\boldsymbol{E}} = (E_x(x, y), E_y(x, y))^{\mathrm{T}}$. By eliminating $\widetilde{\boldsymbol{E}}$, we arrive at

$$\mathrm{curl}((-\mathrm{i}\omega\epsilon + \sigma)^{-1}\, \mathrm{curl}\, H_z) - \mathrm{i}\omega\mu H_z = 0.$$

Suppose $\epsilon = \epsilon_0$ and $\sigma = \sigma_0$, the permittivity and conductivity of the background medium, from which it follows that div $\widetilde{\boldsymbol{E}} = 0$ holds. Consequently, the component H_z satisfies

$$\Delta H_z + (\omega^2\epsilon_0\mu + \mathrm{i}\omega\sigma_0\mu)H_z = 0.$$

By letting $k^2 = \omega^2\epsilon_0\mu_0$, $c_0 = \frac{1}{\sqrt{\epsilon_0\mu_0}}$ and $c = \frac{1}{\sqrt{\epsilon_0\mu}}$, where μ_0 is the permeability of the background medium, we get $\omega^2\epsilon_0\mu = k^2 c_0^2/c^2$. Hence, in the case of $\sigma_0 = 0$, the desired model (1) follows immediately by setting $n = c_0/c$, and it models magnetically inhomogeneous media since the permeability μ is spatially dependent.

References

[1] Angell T S and Kirsch A 2004 *Optimization Methods in Electromagnetic Radiation* (New York: Springer)
[2] Bao G and Li P 2005 Inverse medium scattering for the Helmholtz equation at fixed frequency *Inverse Problems* **21** 1621–41
[3] Cakoni F, Colton D and Monk P 2011 *The Linear Sampling Method in Inverse Electromagnetic Scattering* (Philadelphia: SIAM)
[4] Chen X and Zhong Y 2009 MUSIC electromagnetic imaging with enhanced resolution for small inclusions *Inverse Problems* **25** 015008
[5] Cheney M 2001 The linear sampling method and the MUSIC algorithm *Inverse Problems* **17** 591–5
[6] Colton D and Kirsch A 1996 A simple method for solving inverse scattering problems in the resonance region *Inverse Problems* **12** 383–93
[7] Colton D and Kress R 1998 *Inverse Acoustic and Electromagnetic Scattering Theory* 2nd edn (Berlin: Springer)
[8] Devaney A J 1999 Super-resolution processing of multi-static data using time-reversal and MUSIC available at http://www.ece.neu.edu/faculty/devaney/preprints/paper02n_00.pdf
[9] Gruber F K, Marengo E A and Devaney A J 2004 Time-reversal imaging with multiple signal classification considering multiple scattering between the targets *J. Acoust. Soc. Am.* **115** 3042–7
[10] Hohage T 2001 On the numerical solution of a three-dimensional inverse medium scattering problem *Inverse Problems* **17** 1743–63
[11] Hou S, Solna K and Zhao H 2006 A direct imaging algorithm for extended targets *Inverse Problems* **22** 1151–78
[12] Kirsch A 1998 Characterization of the shape of a scattering obstacle using the spectral data of the far field operator *Inverse Problems* **14** 1489–512
[13] Potthast R 2006 A survey on sampling and probe methods for inverse problems *Inverse Problems* **22** R1–R47
[14] Powell M J D 1981 *Approximation Theory and Methods* (Cambridge: Cambridge University Press)

[15] Schmidt R 1986 Multiple emitter location and signal parameter estimation *IEEE Trans. Antennas Propag.* **34** 276–80

[16] Someda C G 2006 *Electromagnetic Waves* 2nd edn (Boca Raton, FL: CRC Press)

[17] Berg P van den, Broekhoven A L van and Abubakar A 1999 Extended contrast source inversion *Inverse Problems* **15** 1325–44

[18] Zeidler E 1985 *Nonlinear Functional Analysis and Its Applications* (New York: Springer)